

Flat band in hole-doped transition metal dichalcogenide observed by angle-resolved photoemission spectroscopy

Zilu Wang(王子禄), Haoyu Dong(董皓宇), Weichang Zhou(周伟昌), Zhihai Cheng(程志海), and Shancai Wang(王善才)

Citation: Chin. Phys. B, 2023, 32 (**6**): 067103. DOI: 10.1088/1674-1056/acc7f9
Journal homepage: http://cpb.iphy.ac.cn; http://iopscience.iop.org/cpb

What follows is a list of articles you may be interested in

Charge density wave states in phase-engineered monolayer VTe_2

Zhi-Li Zhu(朱知力), Zhong-Liu Liu(刘中流), Xu Wu(武旭), Xuan-Yi Li(李轩熠), Jin-An Shi(时金安), Chen Liu(刘晨), Guo-Jian Qian(钱国健), Qi Zheng(郑琦), Li Huang(黄立), Xiao Lin(林晓), Jia-Ou Wang(王嘉欧), Hui Chen(陈辉), Wu Zhou(周武), Jia-Tao Sun(孙家涛), Ye-Liang Wang(王业亮), and Hong-Jun Gao(高鸿钧)
Chin. Phys. B, 2022, 31 (**7**): 077101. DOI: 10.1088/1674-1056/ac6739

Effect of strain on charge density wave order in α-U

Liuhua Xie(谢刘桦), Hongkuan Yuan(袁宏宽), and Ruizhi Qiu(邱睿智)
Chin. Phys. B, 2022, 31 (**6**): 067103. DOI: 10.1088/1674-1056/ac4f4d

Tri-hexagonal charge order in kagome metal CsV_3Sb_5 revealed by ^{121}Sb nuclear quadrupole resonance

Chao Mu(牟超), Qiangwei Yin(殷蔷薇), Zhijun Tu(涂志俊), Chunsheng Gong(龚春生), Ping Zheng(郑萍), Hechang Lei(雷和畅), Zheng Li(李政), and Jianlin Luo(雒建林)
Chin. Phys. B, 2022, 31 (**1**): 017105. DOI: 10.1088/1674-1056/ac422c

Recent progress on integrating two-dimensional materials with ferroelectrics for memory devices and photodetectors

Jianlu Wang(王建禄), Weida Hu(胡伟达)
Chin. Phys. B, 2017, 26 (**3**): 037106. DOI: 10.1088/1674-1056/26/3/037106

Electronic structures and elastic properties of monolayer and bilayer transition metal dichalcogenides MX_2 (M= Mo, W; X= O, S, Se, Te): A comparative first-principles study

Zeng Fan (曾范), Zhang Wei-Bing (张卫兵), Tang Bi-Yu (唐壁玉)
Chin. Phys. B, 2015, 24 (**9**): 097103. DOI: 10.1088/1674-1056/24/9/097103

RAPID COMMUNICATION

Flat band in hole-doped transition metal dichalcogenide observed by angle-resolved photoemission spectroscopy

Zilu Wang(王子禄)[1,2], Haoyu Dong(董皓宇)[1,2], Weichang Zhou(周伟昌)[3,†], Zhihai Cheng(程志海)[1,2,‡], and Shancai Wang(王善才)[1,2,§]

[1] *Department of Physics and Beijing Key Laboratory of Opto-electronic Functional Materials & Micro-nano Devices, Renmin University of China, Beijing* 100872, *China*

[2] *Key Laboratory of Quantum State Construction and Manipulation (Ministry of Education), Renmin University of China, Beijing* 100872, *China*

[3] *School of Physics and Electronics, Key Laboratory of Low-dimensional Quantum Structures and Quantum Control of Ministry of Education, Key Laboratory for Matter Microstructure and Function of Hunan Province, Synergetic Innovation Center for Quantum Effects and Application, Hunan Normal University, Changsha* 410081, *China*

(Received 23 November 2022; revised manuscript received 22 March 2023; accepted manuscript online 28 March 2023)

Layered transition metal dichalcogenides (TMDCs) gained widespread attention because of their electron-correlation-related physics, such as charge density wave (CDW), superconductivity, etc. In this paper, we report the high-resolution angle-resolved photoemission spectroscopy (ARPES) studies on the electronic structure of Ti-doped 1T-$Ti_xTa_{1-x}S_2$ with different doping levels. We observe a flat band that originates from the formation of the star of David super-cell at the $x = 5\%$ sample at the low temperature. With the increasing Ti doping levels, the flat band vanishes in the $x = 8\%$ sample due to the extra hole carrier. We also find the band shift and variation of the CDW gap caused by the Ti-doping. Meanwhile, the band folding positions and the CDW vector $\boldsymbol{q}_{\rm CDW}$ are intact. Our ARPES results suggest that the localized flat band and the correlation effect in the 1T-TMDCs could be tuned by changing the filling factor through the doping electron or hole carriers. The Ti-doped 1T-$Ti_xTa_{1-x}S_2$ provides a platform to fine-tune the electronic structure evolution and a new insight into the strongly correlated physics in the TMDC materials.

Keywords: transition metal dichalcogenides, charge density wave, electronic structure, angle-resolved photoemission spectroscopy (ARPES)

PACS: 71.20.–b, 71.45.Lr, 71.28.+d **DOI:** 10.1088/1674-1056/acc7f9

1. Introduction

In recent years, transition metal dichalcogenides (TMDCs) have gained wide attention because of their rich electronic phases and unique properties.[1–4] Charge density wave (CDW) and Mott insulator have been observed at low temperatures, and superconductivity has been reported under high pressure.[5] In 1T-TMDC material 1T-TaS_2, a CDW state with $\sqrt{13} \times \sqrt{13}$ reconstruction is formed with a Mott localized electron residing in the center of the star of David (SD). The SD super-cells form a triangular lattice, and quantum spin-liquid states were proposed.[6] In TMDCs, there exist several kinds of interactions, and the instabilities can not be described by a standard mean-field model.[2] The electron–electron correlation should be considered to understand many exotic phenomena, such as the Mott-insulator caused by the existence of the flat band and related physics properties.

Recently, flat bands with high density of states have been observed in the vicinity of Fermi energy ($E_{\rm F}$) by means of scanning tunneling microscopy (STM) in bulk and monolayered TMDC materials.[7,8] With a narrow bandwidth, a considerably small Coulomb interaction or electron–electron correlation could be effective enough to drive many correlation-related quantum phenomena. By tuning the flat band, many exotic phenomena, e.g., metal–insulator transition, could be realized. The flat band in TMDCs provides an ideal platform to study electron-correlated physics on a smaller energy scale.

Among TMDCs materials, the 1T-TaS_2 gained special interests. The crystal structure of 1T-TaS_2 consists of S–Ta–S sandwiches and the tri-layer structure stacks in turns through van der Waals interactions. At the CDW phase, every adjacent 13 Ta atoms form an SD cluster, with an unpaired electron localized at the center Ta of the SD. The SD is interlocked by a triangular superlattice with a periodicity of $\sqrt{13} \times \sqrt{13}$.[9,10] In the SD super-cell, the unpaired electron is reported to be Mott localized at low temperatures.[11–13] These localized electrons are arranged on a triangular superlattice with a geometric frustration, making 1T-TaS_2 a promising candidate for realizing a quantum spin liquid state.[14,15]

The 1T-TaS_2 is sensitive to external perturbations, such as impurity, doping, or pressure.[5,16,17] Superconductivity and Anderson localization have been observed in the Fe-substituted 1T-TaS_2 system.[18] The coexistence of CDW and

†Corresponding author. E-mail: wchangzhou@hunnu.edu.cn
‡Corresponding author. E-mail: zhihaicheng@ruc.edu.cn
§Corresponding author. E-mail: scw@ruc.edu.cn

© 2023 Chinese Physical Society and IOP Publishing Ltd

superconductivity is reported under pressure.[19] In Ti-doped 1T-TaS_2, an anomaly in resistivity peak is found at about 8% doping, and a transition from the CDW phase to an insulating state occurs.[7,20,21] Though much work has been performed on 1T-TaS_2,[2,22–26] the electronic structure measurement on Ti-doped 1T-TaS_2 is still lacking, and the origin of the insulating gap and correlation effect remains puzzled.

In this paper, we report a high-resolution angle-resolved photoemission spectroscopy (ARPES) study on Ti-doped 1T-$Ti_xTa_{1-x}S_2$ ($x = 5\%$ and 8%). We observe a band folding owing to the $\sqrt{13} \times \sqrt{13}$ CDW formation and obtain the CDW vector $\boldsymbol{q}_{\mathrm{CDW}}$. At the 5% Ti doping, we observe the bottom of the flat band originated from the formation of the SD cluster and the CDW gap at low temperatures. With the increase of the Ti-doping ($x = 8\%$), the flat band shifts upward above E_{F}, while the CDW gap still exists at the low temperature. Our results suggest that the filling factor of the flat band could be effectively controlled via hole-doping, such as Ti substitution for Ta. The resistivity anomaly in the phase diagram reported previously could be understood by the disappearance of the flat band near E_{F}. Unveiling the electron structure of the Ti-doped 1T-$Ti_xTa_{1-x}S_2$ will deepen the understanding of strongly correlated physics, such as the metal–insulator transition in the layered materials.

2. Methods

The high-quality 1T-$Ti_xTa_{1-x}S_2$ bulk single-crystals were grown by chemical vapor transport method. Ta (99.99%, Aladdin), $TaCl_5$ (99.99%, Aladdin), S (99.99%, Aladdin), and Ti (99.99%, Aladdin) powders with a nominal molar ratio of 1:1/50:x:2.05 ($x = 0.1\%$, 0.5%, 1%, 2%, 5%, 10%) were mixed thoroughly and then loaded into quartz tubes (inner diameter/outer diameter/length: 14/16/200 mm). 0.15 g iodine (~ 5 mg/cm^3) was added into the quartz tube to acting as the transport agent. The quartz tubes were sealed under high vacuum of 1.33×10^{-3} Pa and then heated in a two-zone furnace for 7 days, where the source and growth temperatures were fixed at 960 °C and 860 °C. The quartz tubes were removed quickly from the furnace and quenched into ice water to obtain the 1T phase. Large 1T-$Ti_xTa_{1-x}S_2$ flakes with size up to 10 mm were collected for further characterization and measurement. X-ray diffraction, scanning electron microscopy, x-ray energy dispersive spectroscopy (EDS) were employed to determine the phase structure, morphology, and composition of the as-prepared samples. The doping content of less than 1% was further calibrated by the relative phase transition temperatures since it is beyond the resolution of EDS. The Ti doping contents of all samples are in good agreement with their nominal molar ratios of source materials, demonstrating the controllable synthesis.

ARPES measurements were performed at the Renmin University of China equipped with a Scienta DA30L analyzer, with a photon energy of 10.05 eV, and the BL03U beamline of Shanghai Synchrotron Radiation Facility. The energy and angular resolutions were set to 10 meV and 0.02 Å^{-1}, respectively. Clean surfaces for ARPES measurements were obtained by *in situ* cleaving the samples. Photoemission spectra presented in this work were recorded from $T = 320$ K to 15 K using the photon energies $h\nu = 23$ eV and 70 eV, in a working ultrahigh vacuum better than 7×10^{-11} Torr.

3. Results and discussion

3.1. Band structure

The crystal structure of 1T-TaS_2 consists of S–Ta–S sandwiches, belongs to $P\bar{3}m1$ space group. With the substitution of Ti for Ta, hole carriers are introduced. Due to the similar ionic radii of Ti and Ta, the system is relatively stable, and no extra structural distortion is found with the Ti doping.[20,27]

The three-dimensional (3D) Brillouin zone (BZ) of 1T-$Ti_xTa_{1-x}S_2$ is shown in Fig. 1(a). Figure 1(b) shows the integrated intensity of $x = 5\%$ within $E_{\mathrm{F}} \pm 20$ meV at high temperature in the incommensurate CDW (IC-CDW) state. Six elliptical Fermi surfaces (FSs) with high intensity around the $\overline{M}$ point are observed. Meanwhile, no spectral intensity at BZ center $\overline{\Gamma}$ is observed. This band structure is similar to the pristine 1T-TaS_2 at normal state.[28] Then we take measurements along the high symmetry line $\overline{\Gamma}$–$\overline{M}$ and show the corresponding intensity and energy distribution curves (EDCs) plot in Figs. 1(c) and 1(d), respectively. From the figure, an electron band disperses towards $\overline{\Gamma}$ and crosses E_{F} at $k_{\parallel} \sim 0.3$ Å^{-1}, which forms the elliptical FS around the $\overline{M}$ point. At the low temperature, the 1T-$Ti_xTa_{1-x}S_2$ enters a near-commensurate CDW phase, which is a mixture of the commensurate and incommensurate domains.[29] The FS topology and the corresponding band dispersion along $\overline{\Gamma}$–$\overline{M}$ are shown in Figs. 1(e)–1(g). Compared to the high-temperature band structure, significant changes are the opening of a band gap and the emergence of a flat band feature near the BZ center. As highlighted in Fig. 1(f), the electron band disperses towards E_{F} and then bends back at the location that corresponds to the $\sqrt{13} \times \sqrt{13}$ reconstructed BZ boundary. In Fig. 1(f), we observe that the flat band is located at the BZ center, and this feature is a result of the isolated electron residing at the center Ta atom of the SD in 1T-TaS_2. As a consequence, the FS topology changes significantly as compared to the high temperature. The elliptical FSs vanish, and high intensity at the BZ center emerges, as shown in Fig. 1(e).

The characteristics of the flat band remain unclear. The pristine 1T-TaS_2 system was previously believed to be in a Mott-insulating state, with band splitting observed in STM.[7]

However, ARPES measurements reported the existence of the lower Hubbard band only within a certain temperature range, and eventually the system became a band insulator at low temperatures.[28] With the introduction of hole carriers, where the filling of the flat band is away from one electron per SD, surprisingly, the splitting feature still exists in STM under spatial average. At $x = 5\%$, which is far from half-filling of a SD and where electron correlation is supposed to be weakened, both weights below and above E_F are observed in STM. This observation raises the question whether the observed flat band is the bottom of an electron band, or a lower Hubbard band if the electron correlation is strong enough to drive the Mott transition. Further detailed ARPES and STM measurements are needed in future studies.

Figures 2(a) and 2(b) show the intensity plot and corresponding second derivative plot along a high symmetry direction ($\overline{\Gamma}$–$\overline{M}'$–$\overline{\Gamma}'$) of the reconstructed BZ, marked as Cut1 in Fig. 1(e). The flat band is observed in the vicinity of E_F, and the CDW gap opens at the reconstructed BZ boundary. From the second derivative plot shown in Fig. 2(b), the folded band owing to the $\sqrt{13} \times \sqrt{13}$ CDW reconstruction is enhanced and better visualized. The band intercepts the shadow band with weaker intensity at the reconstructed BZ boundaries and opens a CDW gap near E_F. We estimate the $\boldsymbol{q}_{CDW}$ by connecting the band crossing points between the main band and the folded band and obtain a value of about 0.6 Å^{-1}, which is consistent with the theoretical value of the $\sqrt{13} \times \sqrt{13}$ reconstruction. Then we schematically illustrate the band folding, the formation of the CDW gaps, and the flat band in Fig. 2(c).

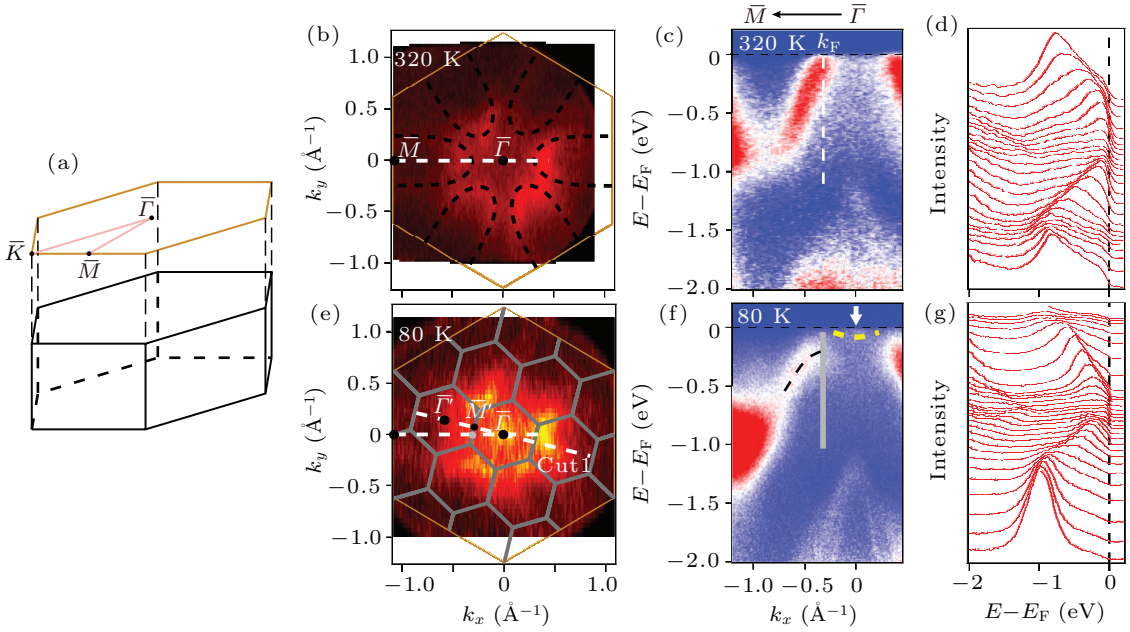


Fig. 1. (a) Three-dimensional BZ and two-dimensional projected BZ of 1T-Ti$_x$Ta$_{1-x}$S$_2$. (b) FS of the 1T-Ti$_{0.05}$Ta$_{0.95}$S$_2$, taken at $T = 320$ K. The elliptical FSs are denoted by black dashed lines. (c), (d) Band spectra and the corresponding EDC along $\overline{\Gamma}$–$\overline{M}$ direction, respectively. (e), (f), (g) same as (b), (c), (d) but taken at $T = 80$ K. The yellow and grey lines depict the BZ and reconstructed BZ, respectively. The bottom of the flat band is marked by a white arrow, and the black dashed line in (f) serves as a guide to the eyes for band dispersion. The grey line in (f) indicates the reconstructed BZ boundary.

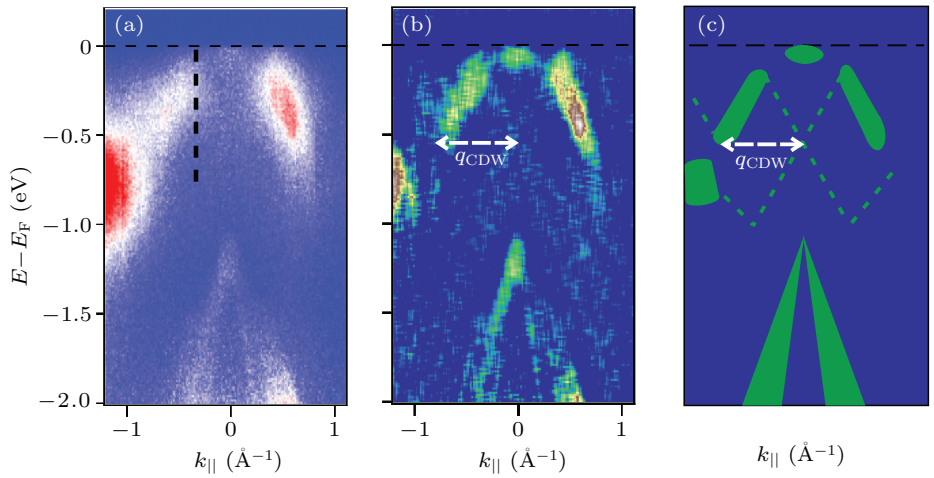


Fig. 2. (a) The band spectra along Cut1 direction from Fig. 1(e). The vertical black line indicates the reconstructed BZ boundary. (b) The corresponding second derivative plot. (c) The sketch with extracted data from (a) and (b). The white arrow presented the $\boldsymbol{q}_{CDW}$.

The ARPES measurement on the 1T-$Ti_xTa_{1-x}S_2$ with 8% Ti doping, which corresponds to one Ti substitution of Ta in a SD super-cell ($1/13 \sim 0.077$), is shown in Fig. 3. Similar to the $x = 5\%$ doping at high temperature, we observe six elliptical FSs around the $\overline{M}$ point in the IC-CDW state, as shown in Fig. 3(a). The intensity plot and EDCs plots along $\overline{\Gamma}$–$\overline{M}$ show an electron band dispersing towards $\overline{\Gamma}$ and across E_F, shown in Figs. 3(b) and 3(c). In the CDW state, the electron band also opens a CDW gap at the reconstructed BZ boundary and shows a band bending. Similar to the $x = 5\%$ sample, the intensity plot shows the disappearance of the elliptical FSs due to the gap opening. However, the higher intensity at the $\overline{\Gamma}$ is not present at this doping level, as shown in Fig. 3(d).

The change in the FS topology with doping could be attributed to the extra hole carriers introduced with Ti substitution for Ta. This is also identified by the extracted band dispersion from the two samples, as shown in Fig. 3(g). From the figure, in the IC-CDW state, the band of the $x = 8\%$ sample is shifted upward in comparison to that of the $x = 5\%$ doping, which is caused by the introduction of hole carriers and the corresponding downshift of the chemical potential. The larger k_F of the $x = 8\%$ sample indicates the shrink of the enclosed area of the six elliptical electron-like FSs, consistent with the Luttinger theorem. As a consequence, the flat band in the CDW state eventually moves above E_F and beyond the ARPES measurements. The disappearance of the flat band near E_F, and the corresponding low energy carriers, will cause a rapid increase of electronic resistivity at this doping region and was reported by transport measurement.[7]

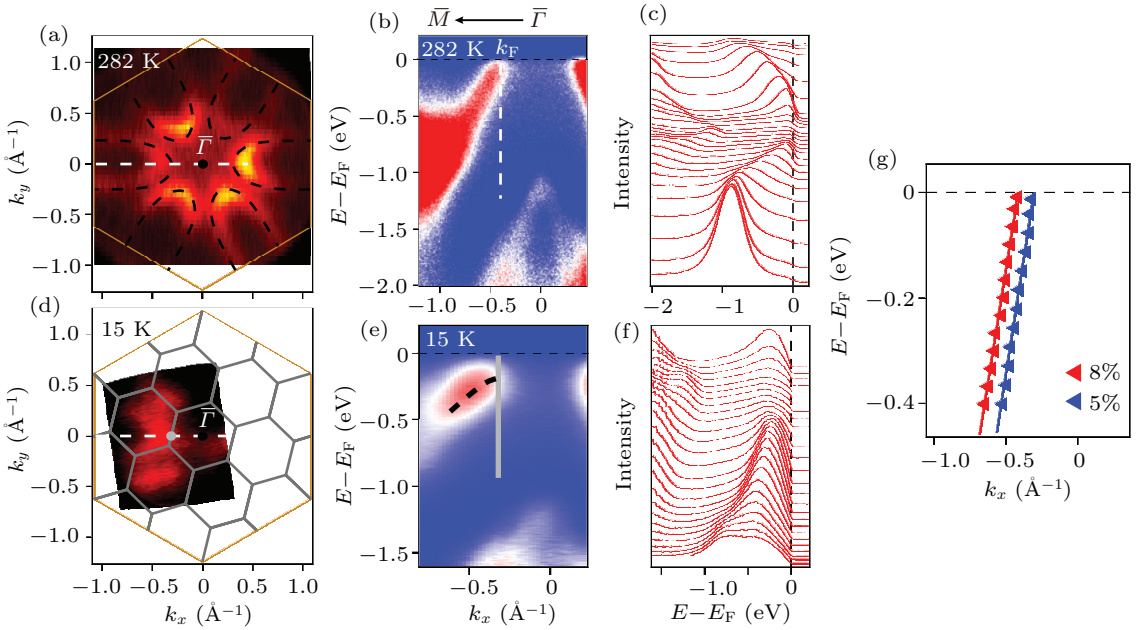


Fig. 3. (a) The FS of 1T-$Ti_{0.08}Ta_{0.92}S_2$ recorded with $h\nu = 70$ eV, taken at $T = 282$ K. (b), (c) Intensity and the corresponding EDCs plots along $\overline{\Gamma}$–$\overline{M}$ direction, respectively. (d)–(f) same as (a)–(c) but with $h\nu = 23$ eV at $T = 15$ K. The black dashed line in (e) is a guide to the eyes for band dispersion, and the grey line indicates the reconstructed BZ boundary. (g) Band dispersion extracted from $x = 5\%$ and 8% samples.

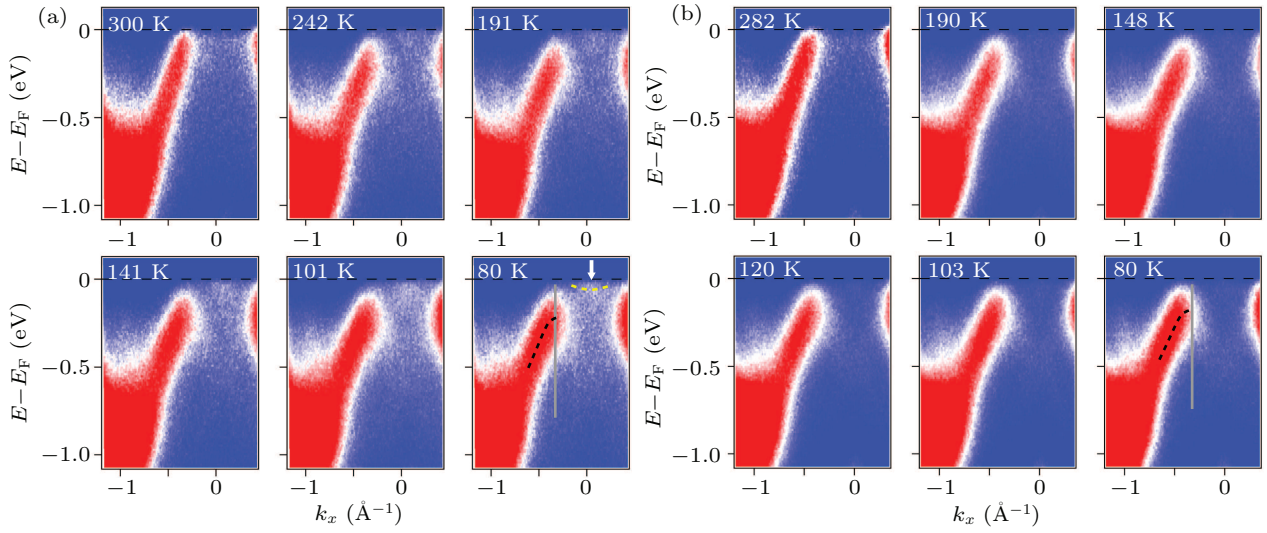


Fig. 4. (a), (b) Temperature-dependent band dispersions of the $x = 5\%$ and 8% samples of 1T-$Ti_xTa_{1-x}S_2$ with $h\nu = 70$ eV along the $\overline{\Gamma}$–$\overline{M}$ direction. The bottom of the flat band and band bending are marked by the yellow and black dashed lines, respectively. The grey line indicates the reconstructed BZ boundary.

Temperature-dependent measurements are taken to investigate the spectral change across the CDW transition. Figure 4 shows the band dispersions along the $\overline{\Gamma}$–$\overline{M}$ direction of 1T-$Ti_xTa_{1-x}S_2$ with $x = 5\%$ and $x = 8\%$ at selected temperatures. For both doping levels, the bands cross E_F at high temperature in the IC-CDW state ($T = 300$ K for $x = 5\%$ and $T = 282$ K for $x = 8\%$), and then start to lose intensity in the vicinity of E_F near the reconstructed BZ boundary with the decrease of temperature. At the lowest temperatures, both $x = 5\%$ and 8% samples show band bendings at the reconstructed BZ boundary and open the CDW gaps. Meanwhile, the flat band feature gradually emerges near E_F at the BZ center at the $x = 5\%$ doped sample, as illustrated in Fig. 4(a). However, the sign of the flat band is lacking during the decrease temperature in the $x = 8\%$ doped sample, as shown in Fig. 4(b).

3.2. Gap in 1T-$Ti_xTa_{1-x}S_2$

Figures 6(a) and 6(b) show the schematic illustration of the bands extracted from the $x = 5\%$ and 8% Ti-doped 1T-$Ti_xTa_{1-x}S_2$ along the $\overline{\Gamma}$–$\overline{M}$ direction at low temperature, respectively. There are three energy scales, Δ_1, Δ_2, and CDW gaps, as illustrated in the figure. To reveal the energy scales during the CDW transition, we take the EDCs at the reconstructed BZ boundary and BZ center $\overline{\Gamma}$ at different temperatures and extract the Δ_1, Δ_2, and CDW gaps. The gaps Δ_1 and Δ_2, defined as the difference between E_F and the top of band bendings, are extracted from the symmetrized EDCs at the reconstructed BZ boundaries for $x = 5\%$ and 8% doped samples, respectively. In Figs. 5(a) and 5(c), the symmetrized EDCs show one peak at a temperature slightly above the CDW transition and two peaks at the temperatures below the transition, supporting the opening of gaps at this momentum through the transition.[20,30] The CDW gap is defined as the difference between the flat band and the top of band bending and extracted from the peaks between the EDCs at the reconstructed BZ boundary (solid lines) and the $\overline{\Gamma}$ point (dashed lines), as shown in Fig. 5(b).

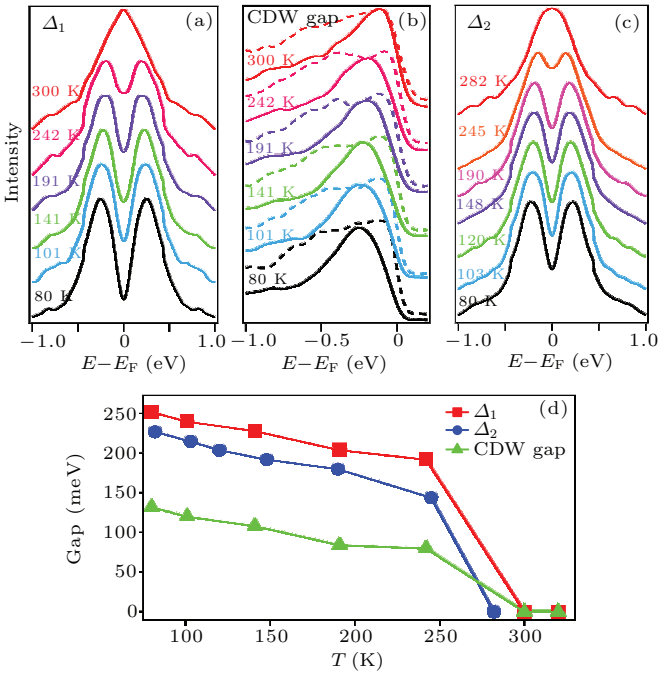


Fig. 5. (a) Symmetrized EDC of $x = 5\%$ sample at reconstructed BZ boundary as marked in Fig. 4(a). (b) EDCs of $x = 5\%$ at $\overline{\Gamma}$ point (dashed lines) and reconstructed BZ boundary (solid lines). (c) Symmetrized EDC of $x = 8\%$ sample at the reconstructed BZ boundary marked in Fig. 4(b). (d) Extracted values of Δ_1, Δ_2, and CDW gaps from (a)–(c) at selected temperatures.

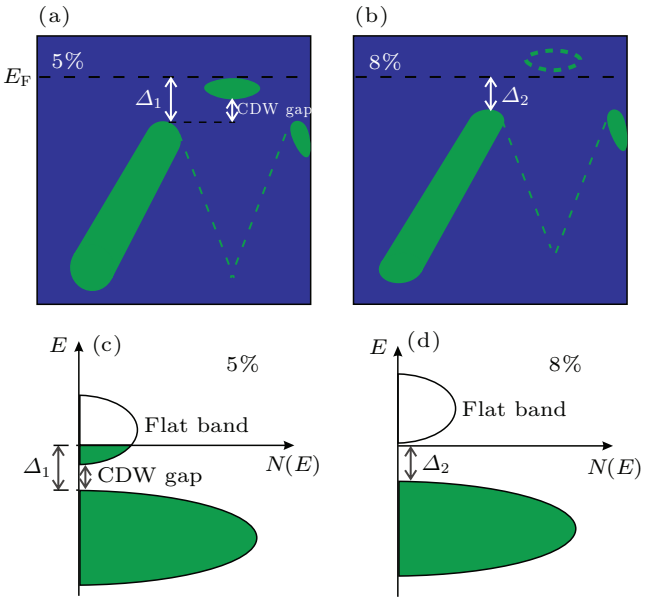


Fig. 6. (a), (b) The sketch of band dispersion of the $x = 5\%$ and 8% samples of 1T-$Ti_xTa_{1-x}S_2$ along the $\overline{\Gamma}$–$\overline{M}$ direction at CDW state, respectively. (c), (d) The schematic illustration of the density of state at $x = 5\%$ and 8% Ti dopings, respectively.

The extracted Δ_1, Δ_2, and CDW gap sizes are summarized in Fig. 5(d). As the temperature decreases through the transition point, the Δ_1, Δ_2, and CDW gaps open and gradually increase. As a comparison, the gap Δ_2 ($x = 8\%$) is smaller than the gap Δ_1 ($x = 5\%$), which is most probably due to the band shift-up with the further increase of the doping level, as shown in Fig. 3(g). The CDW gap is defined as the indirect gap between the top of the band bending and the flat band at $x = 5\%$ doping. For $x = 8\%$ doping, the flat band shifts up above E_F, the CDW gap is estimated by the Δ_2, which gives a smaller value. We find that the CDW gap (Δ_2) in the $x = 8\%$ sample is larger than that in the $x = 5\%$ sample, as seen in Fig. 5(d). It suggests that the CDW gap increases with further Ti-doping, and the CDW strength becomes stronger with the increase of the doping level. With the up-shift of the flat band across E_F, the filling factor of the flat band decreases to zero, and thus the electron correlation driven Mott localization should vanish at $x \geq 8\%$ Ti-doped system. A CDW to insulator transition has been reported at the Ti-concentration of about 8%–10% and is consistent with our result.[7] The filling control of the Mott insulator and its exotic behavior have

been challenging for decades, such as high T_C superconductivity. The delicate fine-tuning of the filling factor of the flat band in this TMDC with a smaller energy scale will provide another testing ground for understanding the electron–electron correlation phenomena, such as Mott-localization and quantum spin liquid behavior.

4. Summary

In summary, we report the electron structure of the Ti-doped 1T-$Ti_xTa_{1-x}S_2$ sample with different doping levels and temperatures by ARPES measurements. In both $x = 5\%$ and $x = 8\%$ dopings, the band bending due to the formation of SD is observed. As the CDW gaps exist in both samples, the bottom of the flat band is only observed at the low temperature in the $x = 5\%$ sample but absent with further doping. The CDW gap in $x = 8\%$ is larger than that in the $x = 5\%$ sample, indicating that the CDW strength becomes stronger with further Ti doping. As the ground state of 1T-TaS_2 remains puzzling due to many kinds of interactions, revealing the electron structure of the doped 1T-TaS_2 family with the variation of temperature and doping will deepen our understanding of the strongly correlated physics in the layered materials and indeed needs more theoretical exploration.

Acknowledgements

Project supported by the National Natural Science Foundation of China (Grant Nos. 12274455, 11774421, 21622304, 61674045, 11604063, and 12074116), the National Key R&D Program of China (Grant Nos. 2016YFA0200700 and 2022YFA1403800), and the Strategic Priority Research Program (Chinese Academy of Sciences, CAS) (Grant No. XDB30000000). Z. H. Cheng was supported by the Fundamental Research Funds for the Central Universities and the Research Funds of Renmin University of China (Grant No. 21XNLG27).

References

[1] Castro Neto A H 2001 *Phys. Rev. Lett.* **86** 4382
[2] Rossnagel K 2011 *J. Phys.: Condens. Matter* **23** 213001
[3] Borisenko S V, Kordyuk A A, Yaresko A N, Zabolotnyy V B, Inosov D S, Schuster R, Büchner B, Weber R, Follath R, Patthey L and Berger H 2008 *Phys. Rev. Lett.* **100** 19640
[4] Fazekas P and Tosatti E 1979 *Philos. Mag. B* **39** 229
[5] Sipos B, Kusmartseva A F, Akrap A, Berger H, Forró L and Tutiš E 2008 *Nat. Mater.* **7** 960
[6] Mañas-Valero S, Huddart B M, Lancaster T, Coronado E and Pratt F L 2021 *NPJ Quantum Mater.* **6** 69
[7] Gao J J, Zhang W H, Si J G, Luo X, Yan J, Jiang Z Z, Wang W, Lv H Y, Tong P, Song W H, Zhu X B, Lu W J, Yin Y and Sun Y P 2021 *Appl. Phys. Lett.* **118** 213105
[8] Lin H, Huang W, Zhao K, Qiao S, Liu Z, Wu J, Chen X and Ji S H 2020 *Nano Res.* **13** 133
[9] Scruby C B, Williams P M and Parry G S 1975 *Philos. Mag.* **31** 255
[10] Fazekas P and Tosatti E 1980 *Physica B+C* **99** 183
[11] Wilson J A, Di Salvo F J and Mahajan S 1975 *Adv. Phys.* **24** 117
[12] Manzke R, Buslaps T, Pfalzgraf B, Skibowski M and Anderson O 1989 *Europhys. Lett.* **8** 195
[13] Pillo T, Hayoz J, Berger H, Fasel R, Schlapbach L and Aebi P 2000 *Phys. Rev. B* **62** 4277
[14] Law K T and Lee P A 2017 *Proc. Natl. Acad. Sci. USA* **114** 6996
[15] He W Y, Xu X Y, Chen G, Law K T and Lee P A 2018 *Phys. Rev. Lett.* **121** 046401
[16] Xue X, Wang X, Song Y and Mi W 2018 *J. Alloys Compd.* **739** 723
[17] Wagner K E, Morosan E, Hor Y S, Tao J, Zhu Y, Sanders T, McQueen T M, Zandbergen H W, Williams A J, West D V and Cava R J 2008 *Phys. Rev. B* **78** 104520
[18] Ang R, Tanaka Y, Ieki E, Nakayama K, Sato T, Li L J, Lu W J, Sun Y P and Takahashi T 2012 *Phys. Rev. Lett.* **109** 176403
[19] Ritschel T, Trinckauf J, Garbarino G, Hanfland M, Zimmermann M V, Berger H, Büchner B and Geck J 2013 *Phys. Rev. B* **87** 125135
[20] Di Salvo F J, Wilson J A, Bagley B G and Waszczak J V 1975 *Phys. Rev. B* **12** 2220
[21] Thompson A H, Pisharody K R and Koehler R F 1972 *Phys. Rev. Lett.* **29** 163
[22] Arita M, Negishi H, Shimada K, Xu F, Ino A, Takeda Y, Yamazaki K, Kimura A, Qiao S, Negishi S, Sasaki M, Namatame H and Tanigu M 2004 *Physica B* **351** 265
[23] Clerc F, Battaglia C, Bovet M, Despont L, Monney C, Cercellier H, Garnier M G, Aebi P, Berger H and Forró L 2006 *Phys. Rev. B* **74** 155114
[24] Qiao Y B, Li Y L, Zhong G H, Zeng Z and Qin X Y 2007 *Chin. Phys.* **16** 3809
[25] Wen W, Dang C H and Xie L M 2019 *Chin. Phys. B* **28** 058504
[26] Hu Q, Yin C, Zhang L L, Lei L, Wang Z S, Chen Z Y, Tang J and Ang R 2018 *Chin. Phys. B* **27** 017104
[27] Zhang W, Gao J, Cheng L, Bu K, Wu Z, Fei Y, Zheng Y, Wang L, Li F, Luo X, Liu Z, Sun Y and Yin Y 2022 *NPJ Quantum Mater.* **7** 8
[28] Wang Y D, Yao W L, Xin Z M, Han T T, Wang Z G, Chen L, Cai C, Li Y and Zhang Y 2020 *Nat. Commun.* **11** 4215
[29] Djurdjić Mijin S, Baum A, Bekaert J, Šolajić A, Pešić J, Liu Y, He Ge, Milošević M V, Petrovic C, Popović Z V, Hackl R and Lazarević N 2021 *Phys. Rev. B* **103** 245133
[30] Chen X M, Miller A J, Nugroho C, de la Peña G A, Joe Y I, Kogar A, Brock J D, Geck J, MacDougall G J, Cooper S L, Fradkin E, Van Harlingen D J and Abbamonte P 2015 *Phys. Rev. B* **91** 245113